

1 **Early maturation** processes in coal.

2 Part 1: Pyrolysis mass balances and structural evolution of coalified wood from the
3 Morwell Brown Coal seam

4
5 Elodie Salmon ^{a,c}, Françoise Behar ^a, François Lorant ^a, Patrick G. Hatcher ^b, Paul-Marie
6 Marquaire ^c.

7 *a Institut Français du Pétrole, BP 311, 92506 Rueil-Malmaison cedex, France*

8 *b Department of Chemistry and Biochemistry, Old Dominion University, Norfolk, VA,*
9 *USA 23529*

10 *c Département de Chimie Physique des Réactions, Institut Polytechnique de Lorraine, 1*
11 *rue Grandville, B.P.20451 F, 54001 Nancy cedex, France.*

12
13 Corresponding author:

14 François Lorant, IFP (Institut Français du Pétrole), Département de Géochimie, 1 et 4 avenue
15 du bois Préau, 92852 Rueil-Malmaison, France, tel : 33 14 752 6910 fax : 33 14 752 7019,
16 email : francois.lorant@ifp.fr
17

18

19
20
21
22
23
24
25
26
27
28
29
30
31
32
33
34
35

Abstract

In this work, we develop a theoretical approach to evaluate maturation process of kerogen-like material, involving molecular dynamic reactive modeling with a reactive force field to simulate the thermal stress. The Morwell coal has been selected to study the thermal evolution of terrestrial organic matter. To achieve this, a structural model is first constructed based on models from the literature and analytical characterization of our samples by modern 1-and 2-D NMR, FTIR, and elemental analysis. Then, artificial maturation of the Morwell coal is performed at low conversions in order to obtain, quantitative and qualitative, detailed evidences of structural evolution of the kerogen upon maturation. **The observed chemical changes are a defunctionalization of the carboxyl, carbonyl and methoxy functional groups coupling with an increase of cross linking in the residual mature kerogen. Gaseous and liquids hydrocarbons, essentially CH₄, C₄H₈ and C₁₄₊ liquid hydrocarbons, are generated in low amount, merely by cleavage of the lignin side chain.**

Keywords: thermal decomposition, Morwell coal, molecular model, coal maturation, lignite.

36 1. **Introduction:**

37 Thermal stress in the Earth's subsurface is one of the most important forces driving
38 hydrocarbon generation from kerogen in shales and coal (Philippi, 1965; Louis **and** Tissot,
39 1967; Albrecht and Ourisson, 1969). For terrestrial material that typically forms coal, the
40 main **hydrocarbon** is methane gas. However, in some cases, coal is considered to be a source
41 of paraffinic-rich hydrocarbons of **molecular weight higher** than methane or volatile
42 hydrocarbon gases (Mukhopadhyay et al., 1991; Fowler et al., 1991, Nelson et al., 1998). Of
43 particular interest in this current study is the origin of methane and other gaseous
44 hydrocarbons, especially from precursor chemical structures like lignin. Previous studies have
45 shown that lignin is an important precursor for coal structures (Hatcher, 1989) and that
46 methane is generated in abundance as the main hydrocarbon from such a structural
47 component of wood during maturation (Behar and Hatcher, 1995). Moreover, here are many
48 kerogens whose organic matter is partly sourced from terrestrially-derived organic matter
49 which contains as its main constituent lignin. Knowing the hydrocarbon-generating potential
50 and mechanism from the lignaceous components of such kerogens is **of paramount interest**
51 to assessing the relative importance of terrestrial organic matter in the overall hydrocarbon
52 potential of these kerogens (**Behar and Hatcher, 1995**).

53 The work reported in the present paper is part of a study that aims at establishing, from
54 a theoretical point of view, the primary cracking mechanism for **insoluble sedimentary**
55 **organic matter** derived exclusively from lignin. This paper addresses the structural study of
56 specific **insoluble sedimentary organic matter** materials and the construction of the
57 corresponding molecular models. We also describe the thermal decomposition, at low
58 conversions, of a sample in which we deduce the initial chemical reactions for conversion.
59 For this purpose, a lignitic wood from the Morwell coal (Victorian brown coal, Australia) was
60 selected as our precursor material, recognizing that it has already undergone some maturation

61 to achieve a coal rank of lignite (**Hatcher, 1988**). This wood sample has previously been
62 shown by flash pyrolysis/gas chromatography/mass spectrometry to contain mainly lignin-
63 derived structures (Behar and Hatcher, 1995). In a previous study, the chemical structural
64 composition and a proposed structural model for gymnospermous wood was presented
65 (Hatcher, 1989). However, a model for angiospermous lignite has yet to be proposed.

66 Our approach is to first compare our chemical analyses to chemical models previously
67 proposed in the literature for similar samples. Based on both literature models and our own
68 analyses, updated chemical structures are proposed for a material derived from
69 angiospermous wood. Closed pyrolysis of the wood in gold tubes followed by a detailed
70 quantitative analysis of the products, including the matured lignite residue, allows for mass
71 balances of products and determination of the overall transformation processes during
72 simulated maturation. Thermal decomposition products are identified using numerous
73 techniques such as elemental analyses, gas chromatography (GC) coupled to flame ionization
74 detection (FID) or thermal conductivity detection (TCD), infrared (IR) spectroscopy, and
75 solid and liquid state ^{13}C NMR.

76

77 **2. Sample: Lignite from the Morwell coal**

78 **The Morwell lignite was collected from the Morwell Open Cut, Latrobe Valley,**
79 **Victoria, Australia and is composed essentially of angiospermous wood transformed to**
80 **the rank of lignite B (Hatcher, 1988; Behar and Hatcher, 1995).** It is part of an entire
81 fossil tree buried at the peat stage in the Early Miocene and coalified within the deposit.
82 During early diagenesis, biodegradation and mild chemical processes led to the
83 decomposition of the cellulose and the hemi-cellulose and transformed the lignin structure
84 into lignite (Spackman and Barghoorn, 1966; Philp et al., 1982; Stout et al., 1988; Hatcher et
85 al., 1989, Hatcher and Clifford, 1997). The sample was freeze-dried and ground to a fine

86 powder with a mortar and pestle and stored under nitrogen gas. **This sample is ideal for this**
87 **study because it is naturally organic rich, no chemical treatment is needed to extract the**
88 **organic matter and it is thermally immature.**

89

90 **3. Experimental**

91 The experimental procedures used in this study have been described in detail by
92 Salmon et al. (**accepted manuscript**). In this previous work, similar experiments were
93 performed on an aliphatic biopolymer, algaenan from *Botryococcus braunii* race L. The
94 structural evolution of the Morwell lignite was performed by characterizing the initial sample
95 and the recovered residues from simulated maturations at various temperatures and times.
96 Elemental analysis (combustion/pyrolysis in a Carlo-Erba system) is used to quantify the
97 proportions of C, H and O. Chemical functional groups are measured by Attenuated Total
98 Reflectance Fourier Transform Infrared (ATR – FTIR) spectroscopy on a Bruker Tenser 27
99 spectrometer.

100 Detailed structural characterizations are obtained by direct polarisation and magic angle
101 spinning (DPMAS) ^{13}C NMR and High Resolution Magic Angle Spinning (HRMAS) NMR
102 techniques on a Bruker AVANCE II Ultra Shield TM 400 MHz spectrometer. Solid-state ^{13}C -
103 NMR spectra were obtained using the basic direct polarization pulse program as described
104 previously (Dria et al., 2002). Approximately 80 mg of sample was inserted into an NMR
105 rotor and spun at the magic angle (54.7°) with a frequency of 15 kHz. A 45 degree pulse angle
106 and a 10 s recycle time were used for each of 10,000 accumulations. Exactly 1024 data points
107 were collected on the free induction decay and an exponential line broadening of 100 Hz was
108 applied prior to Fourier transformation. The spectra were integrated by dropping vertical lines
109 to the baseline between chemical shift regions characteristic of the various types of functional
110 groups.

111 HRMAS spectroscopy was performed with the same NMR spectrometer as described
112 above using a CHN z-axis gradient HRMAS probe. Approximately 20 mg of sample was
113 swelled in DMSO-d₆ (Aldrich, 99.9 atom % D) as it was packed into a 4 mm diameter
114 zirconia MAS rotor spun at the magic angle at 9 kHz. A relaxation delay of 1 s was used for
115 each experiment. A ¹H-¹³C heteronuclear single quantum coherence (HSQC) spectrum was
116 acquired using echo-antiecho gradient selection. In the ¹H dimension (F2), 344 scans were
117 acquired, each collected with 1024 data points for a spectral width of 4,006 Hz (10.01 ppm).
118 In the ¹³C dimension (F1), 128 data points were collected for a spectral width of 166 ppm.
119 Line broadening was used in both dimensions, 1 Hz in the F1 and 0.3 Hz in the F2 dimension.
120 The FIDs were processed in both dimensions using a squared sine multiplication (QSINE)
121 window function.

122 A total correlation spectroscopy (TOCSY) spectrum was acquired with a phase
123 sensitive pulse program that used States-TPPI and the MLEV-17 multiple pulse spin lock
124 sequence. A mixing time of 60 ms was used. A spectral width of 6000 Hz (15 ppm) was
125 obtained in both dimensions. In the F2 dimension, 128 scans were acquired, with 2048 data
126 points. In the F1 dimension, 256 data points were collected and zero-filled to 512. The FIDs
127 were processed in the F2 dimensions using a -3 Hz Gaussian line broadening and in the F1
128 dimension using a line broadening of 1.0 and a QSINE window function. All of the HRMAS
129 spectra obtained on the 400 MHz spectrometer were calibrated using the DMSO peak,
130 referenced to tetramethylsilane (TMS) at 0 ppm.

131 Artificial maturation was performed in gold tube reactors according to methods
132 described by Al Darouich et al. (2006). **Constant temperature confined pyrolysis is**
133 **performed at 200, 225, 250, 275 and 300°C during 9h.** Two tubes were used for each
134 temperature/time condition, one for gaseous product analysis and the other for liquid product
135 analysis. Gas analysis was performed on one gold tube pierced in a vacuum line equipped

136 with a Toepler pump (Behar et al., 1989). Gas chromatography using a thermal conductivity
137 detector was used to characterise and quantify of all the individual gases generated. Two
138 liquid fractions were extracted : the first one recovered the hydrocarbons and the lightest
139 NSOs compounds by pentane extraction, the second one was a dichloromethane extraction for
140 the recovery of most of the heavy hydrocarbons and heteroatom-containing hydrocarbons.
141 Extraction was performed by stirring under reflux for 1 hour. An initial aliquot of the pentane
142 extract was used for quantification of the C₆-C₁₄ compounds. This aliquot was fractionated on
143 a micro column of silica gel into saturated and aromatic compounds. An internal standard (C₂₅
144 *n*-alkane) was added for the quantification by GC-FID. The *n*-C₅ compounds were not
145 quantified because pentane is used as solvent. The second aliquot was evaporated and
146 quantified. A second extraction was performed with dichloromethane (DCM) by stirring
147 under reflux for 1 hour. The DCM extract was evaporated and quantified by weighing. The
148 insoluble residue of this extraction was then dried and weighed. Mass and atomic balances
149 were done in order to check the recovery yield of all the pyrolysis products.

150

151 **4. Results and discussions**

152 *4.1. Initial structure*

153 To our knowledge, no molecular model of the Morwell lignite has been proposed to
154 date in the literature. However a molecular model (Figure 1) of an Australian brown coal (or
155 lignite B) from the Yallourn Open Cut (near the Morwell Open Cut, Holgate, 1985) was
156 proposed by Hatcher (1989) from the experimental data of Bates and Hatcher (1989) and
157 using as a structural motif the lignin model of fresh gymnosperm wood proposed by Alder
158 (1977). This Adler model was transformed by applying experimental observations of
159 peatification and early coalification reactions (Hatcher and Clifford, 1997).

160 We compared the atomic and structural compositions of this gymnosperm coal model
161 with experimental data (elemental and solid-state ^{13}C NMR) obtained on the Morwell lignite
162 (Behar and Hatcher, 1995) that is summarized in Table 1. Results show that, except for the
163 amount of carboxylic groups, the distribution of oxygenated functional groups of the Morwell
164 lignite is very similar to that of the gymnosperm coal model. The major difference is the
165 relative proportion of aliphatic and aromatic carbons. The Morwell lignite is enriched in
166 aliphatic carbon. The Morwell lignite, however, is an angiospermous wood as determined by
167 the flash pyrolysis data shown in Behar and Hatcher (1995). In fact, angiospermous wood
168 contains syringyl based units not found in gymnospermous wood (Philp et al., 1982).
169 Therefore, use of the gymnospermous coal model of Hatcher (1989) is inappropriate to
170 describe the structural nature of the Morwell lignite sample. Hence, we develop a new
171 structural model for Morwell lignite that uses the same approach used by Hatcher (1989) but
172 is derived from the angiospermous lignin structural motif of Nimz (1974) and is constrained
173 by the new experimental data obtained in the current study (elemental analysis, FTIR, and
174 NMR) along with reactions that have been proposed in previous studies (e.g., demethylation,
175 removal of oxygen functional groups from side-chains, aryl ether cleavage-see Hatcher and
176 Clifford, 1997).

177 Reactions of peatification and early coalification have been determined from
178 observations of structural compositions of fresh wood samples and lignitic samples (Stout et
179 al., 1988, Hatcher et al., 1989, Hatcher, 1989, Behar and Hatcher, 1995, McKinney and
180 Hatcher, 1996). Figure 2 summarizes reactions we feel are important in transforming the
181 carbon skeleton of the Nimz lignin model. In order to constrain reaction sites, distances
182 between the reactant functional groups are computed from the coordinates of the individual
183 atoms modeled in 3-D space as described below. Reactions are assumed to occur if the
184 distances are below a distance of three single C-C bonds. Hence the lignin model shown in

185 Figure 3 is constructed to represent the likely structure of the Morwell lignite built around the
186 Nimz motif. We use Cerius² (version 4.8.1, Accerlys software) and minimized our structure
187 with the UFF_VALBOND 1.1 force field (a combination of the original VALBOND method
188 described by Root et al., 1993, augmented with non-orthogonal strength functions taken from
189 Root, 1997 and the Universal Force Field of Rappé et al., 1992) to produce atomic
190 coordinates.

191 With the reactions shown in Figure 2, the carbon skeleton of the Nimz model is
192 rearranged, furan-like structures are removed and the proportion of side-chain hydroxyl/ether
193 groups decreases significantly. Then the proportion of each functional groups are readjusted
194 in the structure to match with quantitative NMR data (Table 2) and better represent the
195 structure of coalified angiospermous wood that is equivalent in rank to the Morwell lignite .
196 Thus, eleven hydroxyl functions are oxidized to carboxyl groups (reaction 6) and two are
197 reduced to yield unsubstituted aliphatic carbons (reaction 7). Twenty methoxy functions are
198 demethylated to yield hydroxyl aryl functions (reaction 8). Dehydroxylation of two hydroxyl
199 aryl groups (reaction 9) allow for the adjustment of the proportions of aryl-O groups. The
200 structural model thusly obtained for the Morwell coal is displayed in Figure 4. This model
201 now serves as the basis for further reactions deduced from artificial maturation in sealed gold
202 tubes. We modify this model in accordance with the chemical analyses of the residue and the
203 liquid and gaseous products.

204

205 *4.2. Observed chemical changes during thermal decomposition of Morwell lignite*

206 As mass balances given in Table 3 show, the total mass loss of the Morwell coal was
207 16.64% at 300 °C exposed for 9 h. The elemental composition changes significantly as
208 demonstrated by the atomic composition of the recovered lignite that exhibits a precipitous
209 decrease of both H/C and O/C ratios with values down to 0.69 and 0.22, respectively.

210 Concurrently, CO₂ is generated at temperatures starting as low as 200 °C, reaching a
211 maximum yield of 12.99 wt% at the most severe conditions and representing 3.6% of the
212 carbon balance. This value is similar to the combined carbon loss from the carboxyl (2.9%)
213 and carbonyl (0.6%) functions as estimated by NMR (Figure 5).

214 4.2.1. Structural evolution observed by DPMAS NMR.

215 We calculate the carbon loss from NMR spectra in Figure 5 by multiplying area
216 percentages for the various integration regions by the total residual carbon from the carbon
217 mass balance that is based on a starting carbon content of 100 mg. Hence, in the structure,
218 17% of the carbonyl functions and 44% of the carboxylic groups are decomposed at 300 °C/9
219 h. The loss of methoxy groups (seen clearly in the NMR spectra of Figure 5) accounts for loss
220 of 5.3% of carbons, but only 0.11 wt% of methane was recovered in gaseous pyrolysis
221 products at the temperature of 300 °C. This lack of correspondence between loss of methoxy
222 groups and methane generation suggests that almost all methoxy species lost are not
223 converted into methane gas. There are multiple possibilities for the formation of end-
224 products: one is that the methyl radical formed reacts with other components of the solid
225 residue, another is reaction of the methyl radical with liquid or volatile products, another is
226 reaction of the methyl radical with OH radical or water to form methanol which is difficult to
227 measure by GC/MS and not included in the mass balance. Considering the uncertainty with
228 which we understand the redistribution of the methyl group, we cannot specifically account
229 for its fate at the moment, but we can suggest that methane is not the only end-product.

230 We cannot exclude the fact that part or the entire yield of the methane originates from
231 pyrolytic degradation of aliphatic carbons in the Morwell coal. Butane, produced in higher
232 yields than methane, is also likely to originate from pyrolytic degradation of aliphatic carbons
233 in the Morwell coal. In fact, we calculate that a combined 2.76 wt% of methane and butane
234 are produced, with no contributions from other volatile hydrocarbon gases. The NMR data

235 shows that 8.22% of aliphatic carbons (CH, CH₂, and CH₃ not including O-substituted
236 aliphatic groups) are lost from the structure of the Morwell coal heated to 300 °C, more than
237 enough to account for the volatile hydrocarbons produced, including methane, if one assumes
238 that aliphatic side chains are the source of these volatile species.

239 If we include O-substituted aliphatic groups and carboxyl/carbonyl species in our
240 carbon balance, there is a substantial loss of lignin side-chain carbons in the Morwell coal
241 considering that the initial sample contained 29% C of total carbons associated with such side
242 chains and the residue contains only 16%. Thus, the carbon skeleton released half of its
243 aliphatic side chains by defunctionalisation and/or depolymerisation and/or pyrolytic
244 degradation.

245 Interestingly, the total amount of aromatic carbons ($fa = \text{aroC} + \text{aryl-O carbons}$) increased by
246 2% (from 64.9% to 66.9% of the carbon). The uncertainty of the peak area in solid-state NMR
247 is estimated to 3% corresponding to a range of uncertainty for the total aromatic carbon of
248 more or less 2%. This suggests that no significant amount of aromatic units is released from
249 the initial structure upon thermal stress. Behar and Hatcher (1995) show that C₆₊ pyrolyzate,
250 extract from residue obtained between 200 and 300°C, is essentially composed of aromatics
251 structures (benzene, phenol, catechol, guaiacol, syringol and naphthalene were identified).
252 Thus, if such structures are formed, they should be recovered in the C₆₊ pyrolyzate. In fact,
253 we measure during the experiment at 300°C during 9h, as low as 0.90wt % of C₆₊ pyrolyzate.
254 Using the atomic composition of the extracts (pentane and DCM C₁₄₊ extract) we can estimate
255 that 0.69% of aromatic carbons are lost which is not significant compared to the uncertainty in
256 area measurements of 2%. This confirms that the amount of aromatic carbon, in the residue
257 recovered at 300°C, is similar to the amount in the initial sample. However, the NMR spectra
258 in Figure 5 show significant changes to the aromatic region. The aryl-O disappears during
259 artificial maturation and the amount that disappears (6.5% of the total carbon) is not exactly

260 equivalent to the amount of aromatic carbon that appears (8.6%) suggesting that aryl-O
261 carbons are transformed to aromatic carbons not bearing an O and that additional aliphatics
262 carbons are converted to aromatic carbons. The proportion of aryl-O functions initially
263 represents 39.8% of total aromatic carbons (*fa*) and these decreases to 28.8% in the recovered
264 residue at 300 °C. Hence, we calculate that 6.55% of carbons correspond to 25% of the aryl
265 functions that are converted into aromatic carbons by losing an oxygen substituent. Two
266 processes may explain the conversion of the aryl-O carbons to aromatic carbons: Behar and
267 Hatcher (1995) demonstrated that two dihydroxyle rings link by an ether group is
268 decomposed to one dihydroxyle units and one monohydroxyle units, another process is that
269 the aryl functions lose an hydroxyl group like by reaction 9.

270 Considering that the total loses of aryl function is decomposed by deshydroxylation of
271 aryl-OH functions forming water and that lost of hydroxyl groups in the lignin side chain
272 generated water, the maximum of carbon involving in dehydration of the mature sample is
273 estimated to 8.2% C (6.5 % of aryl-O carbons + 1.7% of alkoxy carbons) during artificial
274 maturation.

275 4.2.2. *Structural evolution observed by FTIR spectroscopy*

276 In agreement with the solid state NMR, the infrared spectra Figure 6 show a sharp
277 decrease of the C=O and C-O bands relative to the defunctionalisation of the side chain. Only
278 vibration bands of the aromatic skeletons and of OH are observed in the spectra at 300°C.
279 Because of conversion of aryl-O carbons to aromatic carbon, noticed by quantitative NMR,
280 bi- (guaiacol units) and trihydroxyl (synringol) rings are converted in bi- (guaiacol) and
281 monohydroxyl (p-hydroxyphenol) rings suggested for instance in Hatcher et al. (1989).
282 Asymmetric deformation bands at 1470 cm⁻¹ of the aromatic skeleton are replaced by
283 symmetric deformation bands at 1370 cm⁻¹, in the infrared spectra. This change in vibration

284 band is in agreement with the conversion of the syringol and guaiacol asymmetric units into
285 symmetric units of p-hydroxyphenol.

286 4.2.3. *Structural evolution observed by HRMAS NMR*

287 The HRMAS data shown in Figure 7 and 8 for both the unreacted Morwell coal and
288 the residue at 300 C/9h provide additional clues as to the specific transformations that occur
289 during artificial maturation, except for the aromatic region. In the aromatic region of the
290 HSQC spectra (Figure 7 and 8) the cross peaks for both the untreated and matured samples
291 are dispersed over a wide chemical shift range and it is almost impossible to assign any one
292 cross peak to a specific structure. It is apparent that the number of cross peaks diminishes
293 with increasing maturation, and this may be due to the fact that aromatic rings are becoming
294 deprotonated as the result of heating. Once deprotonated the cross peaks for aromatic carbons
295 disappear. On the DPMAS spectra, depicted as a projection on the ordinate, the amount of
296 aromatic carbon protonated represent a small amount of the total area ascribed to aromatic
297 carbons. It is important to underline that those small amount do not represent the precise
298 amount of aromatic carbons protonated but the minimum of those protonated carbons detected
299 by HSQC NMR.

300 In HRMAS spectra quaternary carbons, such as ketone and carboxyl carbons, are not
301 detected, thus only the aldehyde, hydroxyl and methoxy oxygenated functional groups are
302 observed (Figure 7). Aldehyde functional groups, identified as 1, are observed in both
303 TOCSY spectra (Figure 9) of the untreated and the mature sample which show that aldehydes
304 persist upon thermal decomposition at 300 °C. However those aldehydes are not be present in
305 large amounts, because no signal is detected in the region of the carbonyl groups in the HSQC
306 spectra despite the fact that around 3% are quantified by solid state NMR in the initial coal
307 and the residue recovered at 300°C. This suggests that carbonyl groups are mainly ketones
308 which do not show signals in HSQC or TOCSY spectra.

309 In standard lignin structural units, the hydroxyl functions may be substituted in the α ,
310 β or γ positions of the aliphatic side chain (see Figure 1b). Though, in the initial structure only
311 hydroxyl functions in the γ position are observed (cross peak 5 in Figure 7, and 8). We cannot
312 exclude the fact that, α and β hydroxyl functions fall below the detection threshold. In fact,
313 0.4% of hydroxyl functions are quantified in the DPMAS spectrum of the recovered residue
314 whereas in the 2D spectra (HSQC and TOCSY) no signal is observed for these structures. As
315 observed in quantitative NMR spectrum, the intensity of methoxy functional groups assigned
316 to signal 6 is significantly decreased compared to the original coal sample.

317 Aliphatic carbons (Figure 8) are assigned to regions 7, 8, 9 corresponding to $-\text{CH}-$, $-\text{CH}_2-$, and $-\text{CH}_3$. In region 7, additional signals (7B, 7C) appear in the residue recovered at
318 300°C and signal 7A, ascribed to $-\text{CH}-$ in benzylic positions, is detected in both the initial
319 sample and the heated residue. The increase of aliphatic $-\text{CH}-$ groups in the heated residue is
320 probably associated with increased cross linking of the aliphatic side chains. In region 8 of the
321 unheated sample, cross peaks are dispersed and of low intensity, whereas, in the mature
322 sample, cross peaks are well defined, more intense, and less abundant. This is consistent with
323 a process involving defunctionalisation of the aliphatic side chains, a process described
324 previously for the early coalification process (Hatcher and Clifford, 1997; Solomon et al.,
325 1988). In the unheated sample containing mainly lignin structural units, aliphatic carbons ($-\text{CH}-$, $-\text{CH}_2-$ and $-\text{CH}_3$) are typically adjacent to carbons substituted by carboxyl, carbonyl and
326 hydroxyl groups. This can explain why their chemical shifts are broadly dispersed in the
327 spectrum. Upon thermal stress, oxygenated functional groups are released, leading to an
328 increasing signal strength for aliphatic carbons and to more uniform structural characteristics
329 which translate to fewer peaks. Similarly, the TOCSY spectrum (Figure 9 and 10) of the
330 unheated sample contains more dispersed aliphatic cross peaks than the heated sample
331 confirming that aliphatic carbons are less diverse in structural makeup following the artificial

334 maturation. Cross peak 8A is assigned to benzylic CH₂ on the aliphatic side chains and
335 carbons 8B and 8C are attributed to CH₂ groups that are β or γ to the aromatic carbons. The
336 ¹H chemical shifts of peaks in region 8B are more downfield than the ¹H chemical shifts of
337 peaks 8C suggesting that 8B structures are more proximal to aromatic rings or to oxygenated
338 functions than are 8C structures. Increased heating leads to a shift in peaks of region 8B to
339 lower ¹H chemical shift values. Defunctionalisation of the side chain is probably responsible
340 for this change. The transformation of structures associated with 8D (unheated sample) to 8D'
341 (heated sample) is attributed to a rearrangement of the side chain carbons to form a 7-member
342 alicyclic structure as shown in Figure 8, structure V. The broadening of cross peak 8D' is
343 consistent with the presence of the naphthenic structures linked to aromatic rings as shown in
344 Figure 8, structures IX and X. The aromatic naphthenes are also consistent with the evolution
345 of vibrations bands in the infrared spectrum of the heated sample (see discussion above). An
346 increased abundance of methyl groups (region 9) is observed in the spectra of the residue
347 recovered at 300°C. Signals associated with box 9A' correspond to methyl groups in terminal
348 positions on the propyl or ethyl side chains. Peaks in box 9B are assigned to methyl groups in
349 benzylic positions, an indication that part of the original aliphatic lignin side chains has been
350 cleaved.

351 The TOCSY spectra are shown in Figures 9 and 10 and a table of spectral assignments
352 is also given in Figure 10 for protons in the aliphatic region. The information obtained from
353 these spectra is entirely consistent with what is observed in the HSQC spectra; except that a
354 peak is observed for aldehyde protons (1') in the heated coal (Figure 9). This is due to the
355 higher sensitivity of the TOCSY than the HSQC method. In the aromatic region (Figure 9),
356 ¹H-¹H couplings decrease because the amount of protonated aromatic carbons decreases in the
357 structure (see discussion of HSQC NMR data above). In the aliphatic region (Figure 10), only
358 CH₃-CH₂ and CH₂-CH₂ couplings are detected in both spectra. The absence of peaks J_B and

359 J_D in the spectrum of the initial sample shows that the amount of coupling through two and
360 three bonds is very low. This confirms that CH, CH₂ and CH₃ are widely dispersed in the
361 structure and that carbons substituted by oxygenated functional groups disrupt long range
362 connectivity within a single spin system. The cross peak J_H , appearing only in the thermally
363 stressed sample, is assigned to ethyl side chains on aromatic rings which is in agreement with
364 the DPMAS NMR data showing that pyrolytic degradation of the aliphatic side chains occurs
365 during thermal stress.

366

367 5. Overall processes of maturations

368 **The changes in molecular-level composition are globally quantified by elemental**
369 **analysis and solid state NMR, providing constraints for the chemical transformation of**
370 **the lignin model to the rank of lignite. In addition to gaseous and liquids products**
371 **derived from artificial maturation, structural evolution of the coalified wood model is**
372 **described. The carbon balance and thermal decomposition processes are summarized in**
373 **Figure 11. Pyrolysis experiments, performed at 300°C over a period of 9h, convert**
374 **10.6% of the Morwell coal carbon into gaseous and liquid products. Early**
375 **transformations involve mainly the rearrangement of the coal, and generation of**
376 **gaseous products as described previously by Solomon et al. (1988) as well as Behar and**
377 **Hatcher (1995). First, a large amount of CO₂ is generated; then, gaseous hydrocarbons**
378 **are produced in lower amounts. As much CO₂ (5.8% of carbon) is released by**
379 **defunctionalisation as is generated as gaseous and liquid hydrocarbons (4.8% totally as**
380 **methane, butane and C₁₄₊ liquid hydrocarbons). NMR data confirm that CO₂ is formed**
381 **by defunctionalisation of carboxyl and carbonyl functional groups. The methane**
382 **generated is insufficient to be associated with the loss of methoxy groups in NMR**
383 **spectra (5.3% of carbons). At low maturation levels, methyl radicals, presumably**

384 derived from removal of methoxy groups, may be involved in multiple reaction
385 pathways forming various pyrolytic products as well as solid, liquid or gaseous
386 hydrocarbons. Alternatively, methoxy groups may form methanol or formaldehyde,
387 both of which could not be measured directly in this study. Methane and butane could
388 derive from reactions of methyl radicals but they also could evolve from pyrolytic
389 degradation of the aliphatic side chains in lignin. This process could involve
390 defunctionalisation of the side chain followed by pyrolysis.

391 Thermal evolution of the insoluble portion of the coal leads to an increase in cross
392 linking and in the presence of symmetric aromatic structures. This process is in
393 complete agreement with the cross-link processes at low temperature proposed by
394 Solomon et al. (1990) who suggested that, at low temperature and prior to tar evolution,
395 cross linking of the kerogen is correlated to CO₂ loss, water and light hydrocarbons
396 generation. We determined by quantitative NMR that half of the side chains
397 disappeared by formation of gaseous products (CO₂, methane and butane).

398 Behar and Hatcher (1995) have shown that the liquid C₁₄₊ fraction contains
399 aromatic structural units. However, these are minor as our carbon balance indicates
400 that they represent only 1.1% of the carbon. This suggests that aromatic rings in the
401 residue are not significantly lost. Characterization by HRMAS NMR of the mature
402 sample shows that linkages between the aromatic rings and the aliphatic side chains
403 increase but do not enhance the aromaticity of the structure. Oxygenated and
404 protonated carbons on the aromatic rings are converted to carbon-carbon linkages and
405 the proportion of CH increases in the side chains. The proportion of naphthenic rings
406 seems to increase upon maturation, perhaps because of the alteration of the linear side
407 chains.

408

409 **6. Conclusions**

410 This paper is part of a study that seeks to define the relative importance of
411 defunctionalisation and cracking processes during early thermal decomposition of fossil
412 organic matter from numerous sources. Understanding and quantifying those processes is
413 paramount to developing improved kinetic models that are used to evaluate the extent of
414 petroleum generation in sedimentary basins. This paper examines the early reactions for the
415 thermal evolution of a Type III kerogen using as a starting point the chemistry of a sample
416 derived from coalified wood collected from the Gippsland Formation, Morwell open cut mine
417 in Victoria, Australia. The experimental data obtained from artificial maturation in a closed-
418 system reactor will be used for comparison with results of a joint study that proposes use of a
419 new technique for determining maturation changes, that of molecular dynamics simulations
420 with a reactive force field. The structural model for the Morwell coal proposed in this paper
421 (Figure 4) is the only input data of the molecular dynamics simulations. For this reason, the
422 lignin model of Nimz, (1974) is selected to represent the angiospermous origin of the
423 Morwell sample.

424 All the structural changes mentioned in this paper lead to a rearrangement of the coal
425 that can be described through a molecular model that is the subject of a future paper. We
426 expect in this future study to reproduce by molecular dynamic simulations the chemical
427 processes experimentally observed in the current paper in order to validate the simulation
428 procedure and to confirm, from a theoretical point of view, reactions processes proposed here
429 and in the literature. In a way, positive results from the dynamic simulations will also validate
430 the structural model for the Morwell coal.

431

432

433

434

Acknowledgements

435 The experimental facilities used for this research were provided by the IFP (Institut Français
436 du pétrole), and the College of Sciences Major Instrumentation Cluster in Old Dominion
437 University. Fellowship support was provided by the ANRT (Association Nationale de la
438 Recherche Technique), CIFRE grant #458/2004.

439 The authors would like to thank Isaiah Ruhl for assistance with the NMR experiments. We
440 also thank Neal Gupta (Department of EAPS- MIT) and anonymous reviewer for their
441 constructive review of this manuscript.

442

References

443 Adler, E., 1977. Lignin chemistry- Past, present and future. *Wood Science and Technology*.
444 11, 169-218.

445 Albrecht, P., Ourisson, G., 1969. Triterpene alcohol isolation from oil shale. *Science*, 166,
446 1192-1193.

447 Al Darouich, T., Behar, F., Largeau, C., 2006. Thermal cracking of the light aromatic fraction
448 of Safaniya crude oil - Experimental study and compositional modeling of molecular classes.
449 *Organic Geochemistry* 37, 1130-1154.

450 Bates, A. L., Hatcher, P. G., 1989. Solid-state ¹³C NMR studies of a large fossil gymnosperm
451 from the Yallourn Open Cut, Latrobe Valley, Australia. *Organic geochemistry*.14, 6, 609-617.

452 Behar, F., Hatcher, P.G., 1995. Artificial Coalification of a fossil wood from Brown Coal by
453 confined system pyrolysis. *Energy & Fuels* 9, 984-994.

454 Behar, F., Leblond, C., Saint-Paul, C., 1989. Analyse quantitative des effluents de pyrolyse en
455 milieu ouvert et fermé. *Oil and Gas Science and Technology* 44, 387-411.

456 Dria, K. J., Sachleben, J. R., Hatcher, P. G., 2002. Solid-state carbon-13 nuclear magnetic
457 resonance of humic acids at high magnetic field strengths. *Journal of Environmental Quality*,
458 31, 393-401.

459 Fowler, M. G.; Gentzis, T.; Goodarzi, F.; Foscolos, A. E., 1991. The petroleum potential of
460 some Tertiary lignites from northern Greece as determined using pyrolysis and organic
461 petrological techniques. *Organic Geochemistry*, 17, 805-826.

462 Hatcher P. G., Lerch III, H. E., Bates, A. L., Verheyen, T.V., 1989. Solid-state ¹³C nuclear
463 magnetic resonance studies of coalified gymnosperm xylem tissue from Australian brown
464 coals. *Organic Geochemistry*.14, 2, 145-155.

465 **Hatcher, P.G., 1988. Dipolar-Dephasing ¹³C NMR Studies of Decomposed Wood Structure
466 and Changes Associated with Defunctionalization of Lignin Structural Units during
467 Coalification and Coalified Xylem Tissue: Evidence for Chemical. *Energy & Fuel*, 48-58.**

468 Hatcher, P. G., 1989. Chemical structure models for coalified wood (vitrinite) in low rank
469 coal. *Organic Geochemistry* 16, 959-968.

- 470 Hatcher, P. G., Clifford, D. J., 1997. The organic geochemistry of coal: from plant materials to
471 coal. *Organic Geochemistry* 27, 251-274.
- 472 Hatcher, P.G., Wilson, M.A., Vassallo, A.M., Lerche III, H. E., 1989. Studies of
473 angiospermous wood in Australian brown coal by nuclear magnetic resonance and analytical
474 pyrolysis: new insights into the early coalification process. *International Journal of Coal*
475 *Geology* 13, 99-126.
- 476 Holdgate, G. R., 1985. Latrobe Valley Brown Coals_ Their geometry and facies equivalents as
477 a guide to depositional environment. *Australian Coal Geology* 5, 53-68.
- 478 Louis M., Tissot B., 1967. Influence de la température et de la pression sur la formation des
479 hydrocarbures dans les argiles à kérogène. 7th World Petroleum Congress, Mexico, 2, 47-60.
- 480 Mukhopadhyay, P. K., Hatcher, P., Calder, J. H., 1991. Hydrocarbon generation from deltaic
481 and intermontane fluviodeltaic coal and coaly shale from the Tertiary of Texas and
482 Carboniferous of Nova Scotia. *Organic Geochemistry* 17, 765-783.
- 483 Mc Kinney, D. E., Hatcher, P.G., 1996. Characterization of peatified and coalified wood by
484 tetramethylammonium hydroxide (TMAH) thermochemolysis. *International Journal of Coal*
485 *Geology* 32, 217-228.
- 486 Nelson, C. R., Li, W., Lazar, I. M., Larson, K. H., Malik, A., Lee, M. L., 1998. Geochemical
487 Significance of n-Alkane Compositional-Trait Variations in Coals. *Energy & Fuels* 12, 277-
488 283.
- 489 Nimz, H., 1974. Beech lignin-proposal of a constitutional scheme. *Angewandte Chemie*
490 *International Edition, England* 74, 313_321
- 491 Payne, D. F., Ortoleva, P. J., 2002. A model for lignin alteration—part I: a kinetic reaction-
492 network model. *Organic Geochemistry* 32, 1073-1085.
- 493 Philippi, G.T., 1965. On the depth, time and mechanism of petroleum generation. *Geochimica*
494 *and Cosmochimica Acta* 29, 1021-1049.
- 495 Philp, R. F., Gilbert, T. D., and Russell, N. J., 1982. Characterization of Victoria brown coals
496 by pyrolysis techniques combined with gas chromatography and gas chromatography-mass
497 spectrometry. *Australian Coal Geology* 4, 228-243.
- 498 Rappé, A.K., Casewit, C.J., Colwell, K.S., Goddard III, W.A. and Skid, W.M., 1992. UFF, a
499 full periodic table force field for molecular mechanics and molecular dynamics simulations.
500 *Journal of American Chemical Society*, 114, 10024-10039.
- 501 Root, D.M., Landis, C.R. and Cleveland, T., 1993. Valence Bond Concepts Applied to the
502 molecular mechanics description of molecular Shapes. 1. Application to nonhypervalent
503 molecules of the P-block. *Journal of American Chemical Society* 115, 4201-4209.
- 504 Root, D.M., 1997. Ph.D. thesis, University of Wisconsin, Madison, USA.
- 505 Salmon, E., Behar, F., Lorant, F., Hatcher, P.G., Metzger, P., Marquaire, P-M., 2008 accepted
506 manuscript. Thermal decomposition process in algaenan of *Brotryococcus braunii* race L.
507 Part1: Experimental data and structural evolution. *Organic Geochemistry*, *accepted*
508 *manuscript*.
- 509 Solomon P.R., Hamblen D.G., Carangelo R.M., Serio M.A., Deshpande G.V., 1988. General
510 model of coal devolatilization. *Energy and Fuels*, 2, 405-422.
- 511 Solomon, P. R., Serio, M.A., Deshpande, G.V., Kroo, E., 1990. Cross-linking reactions during
512 coal conversion. *Energy & Fuels* 4, 42-54.

- 513 Spackman, W., Barghoorn, E.S., 1966. Coalification of woody tissue as deduced from a
514 petrographic study of Brandon lignite. *Coal Science. American Chemical Society Adv.* 55,
515 695-707.
- 516 Stout, S. A., Boon, J. J., Spackman, W., 1988. Molecular aspects of peatification and early
517 coalification of angiosperm and gymnosperm wood. *Geochimica. Cosmechimica Acta* 52,
518 405-414.
- 519

520 **Table captions**

521

522 **Table 1.** Comparison of the structural composition of the Morwell sample (Behar and Hatcher
523 1995) with that of the brown coal model of Hatcher (**1989**).

524

525 **Table 2.** Structural composition of the fresh lignin model (Nimz, 1974) and of the model and
526 sample of the Morwell coalified wood.

527

528 **Table 3.** Mass and atomic balances of the experimental thermal decomposition of the
529 Morwell coal.

530

531 **Figure captions**

532

533 **Figure 1.** (a) Brown coal molecular model from Hatcher (1990). (b) Typical units in lignin :
534 numbering convention

535 **Figure 2.** Early diagenesis reactions selected to transform the lignin structure to mature rank
536 of lignite. (Hatcher, 1989; Hatcher and Clifford, 1997; Payne and Ortoleva, 2002)

537 **Figure 3.** Beech lignin model from Nimz (1974)

538 **Figure 4.** Structural model of the Morwell sample at coal rank of lignite.

539 **Figure 5.** DPMAS ^{13}C NMR data of the initial sample of Morwell lignite (A) and residue (B)
540 recovered after thermal stress (300°C/9h). The inset table provides quantitative measurements
541 of the relative contributions of the various carbons. The % loss of carbon during artificial
542 maturation is also indicated. The errors (\pm) are given for each calculated value and represent a
543 relative error of 3% for peak area measurements.

544 **Figure 6.** FTIR spectra of the initial sample of Morwell lignite (A) and the residue (B)
545 recovered after thermal stress (300 °C/9 h). Various assignments for stretching (ν) and
546 deformation (δ) frequencies.

547 **Figure 7.** HSQC spectra of the initial sample of Morwell lignite and the residue recovered after
548 thermal stress (300 °C/9 h). Boxed out regions are discussed in the text. The solvent peak is for
549 DMSO. The left ordinate projection is the respective DPMAS ^{13}C NMR spectrum.

550 **Figure 8.** Extended aliphatic region of the HSQC NMR spectra in Figure 9 of the initial
551 Morwell lignite and the residue recovered at 300°C/9 h. Structural assignments for the indicated
552 carbon are presented in a table below of the spectra.

553 **Figure 9.** TOCSY spectra of the initial Morwell lignite and the residue recovered at 300°C/9
554 h. Structural assignments for some cross peaks are listed in Figure 8. Boxed out regions are
555 discussed in the text. The solvent peak is for DMSO.

556

557 **Figure 10.** Expanded view of the TOCSY spectrum in Figure 9. Structural assignments for the
558 ^1H s are presented in a table below of the data with chemical shifts indicated for each coupled
559 system.

560

561 **Figure 11.** Carbon mass balance of the Morwell lignite sample during 300°C/9h closed pyrolysis.

562

563 **Table 1.** Comparison of the structural composition of the Morwell sample (Behar and Hatcher
 564 1995) with that of the brown coal model of Hatcher (1989).

chemical type	Morwell Sample (Behar et al. 1995)	Brown coal Model (Hatcher 1989)
	atomic C (%)	
C=O	2.90	2.78
COOH	4.00	1.85
C _{aro} -OR ₁	22.80	21.30
C _{aro} -	39.50	45.37
O-CH ₃	3.10	4.63
C-O-R ₂	4.00	5.56
-CH, -CH ₂ , -CH ₃	23.10	18.52
total	99.40	100.01
<i>f_a</i>	62.30	66.67
formula	-	C ₁₀₈ H ₁₀₂ O ₃₄
H/C	0.89	0.94
O/C	0.33	0.31

565

566

f_a: aromaticity, R₁ : H or -CH₃, R₂: H, -C-

567

568

569 **Table 2.** Structural composition of the fresh lignin model (Nimz, 1974) and of the model and
 570 sample of the Morwell coalified wood.

chemical structure	Lignin Model	Morwell Model	Morwell Sample
	% C	% C	% C
-C=O	3.1	3.0	3.5
-COOH	0.4	6.4	6.6
-Caro-OR ₁	22.8	24.4	25.8
=Caro-	35.1	39.7	39.1
-C-O-R ₂	18.9	3.0	2.1
-O-CH ₃	13.1	6.0	6.1
-CH, -CH ₂ , -CH ₃	6.6	17.5	16.9
total	100.0	100.0	100.0
<i>fa</i>	57.9	64.1	64.9
Formula	C ₂₅₉ H ₃₀₆ O ₉₃	C ₂₃₄ H ₂₁₆ O ₉₆	
H/C	1.18	0.92	0.94
O/C	0.359	0.410	0.390

571

572

fa: aromaticity, R₁ : H or -CH₃, R₂: H, -C-

573

574

575

576

577 **Table 3.** Mass and atomic balances of the experimental thermal decomposition of the
 578 Morwell coal.

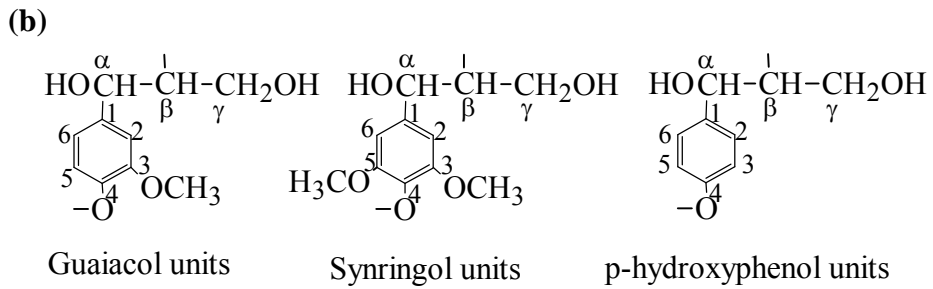
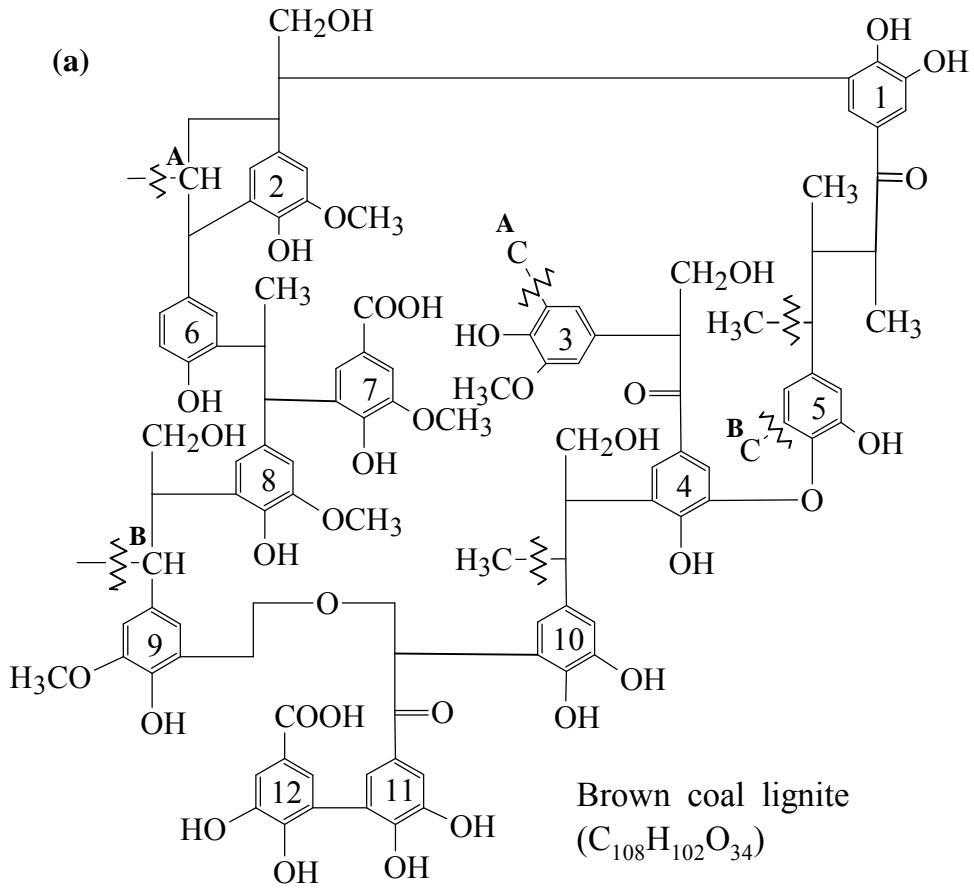
T	t	CO ₂	CH ₄	C ₄	C ₇ -C ₁₄	C ₁₄ +			Residue		
						n-C ₅	DCM	Total	yield	H/C	O/C
°C	h	mg/g							mg/g	atomic ratio	
initial										0.94	0.39
200	9	45.8	< 0.1	2.5	< 0.1	1.3	2.6	52.2	947.8	0.88	0.34
225	9	66.5	< 0.1	4.6	< 0.1	1.4	4.0	76.5	923.5	0.86	0.31
250	9	93.2	0.1	5.5	< 0.1	1.4	6.5	106.7	893.3	0.80	0.29
275	9	105.7	0.4	8.7	< 0.1	1.4	6.2	122.4	877.6	0.73	0.26
300	9	129.9	1.1	26.5	< 0.1	1.7	7.2	166.4	833.6	0.69	0.22

579

580

581

582 **Figure 1.** (a) Brown coal molecular model from Hatcher (1990). (b) Typical units in lignin :
 583 numbering convention



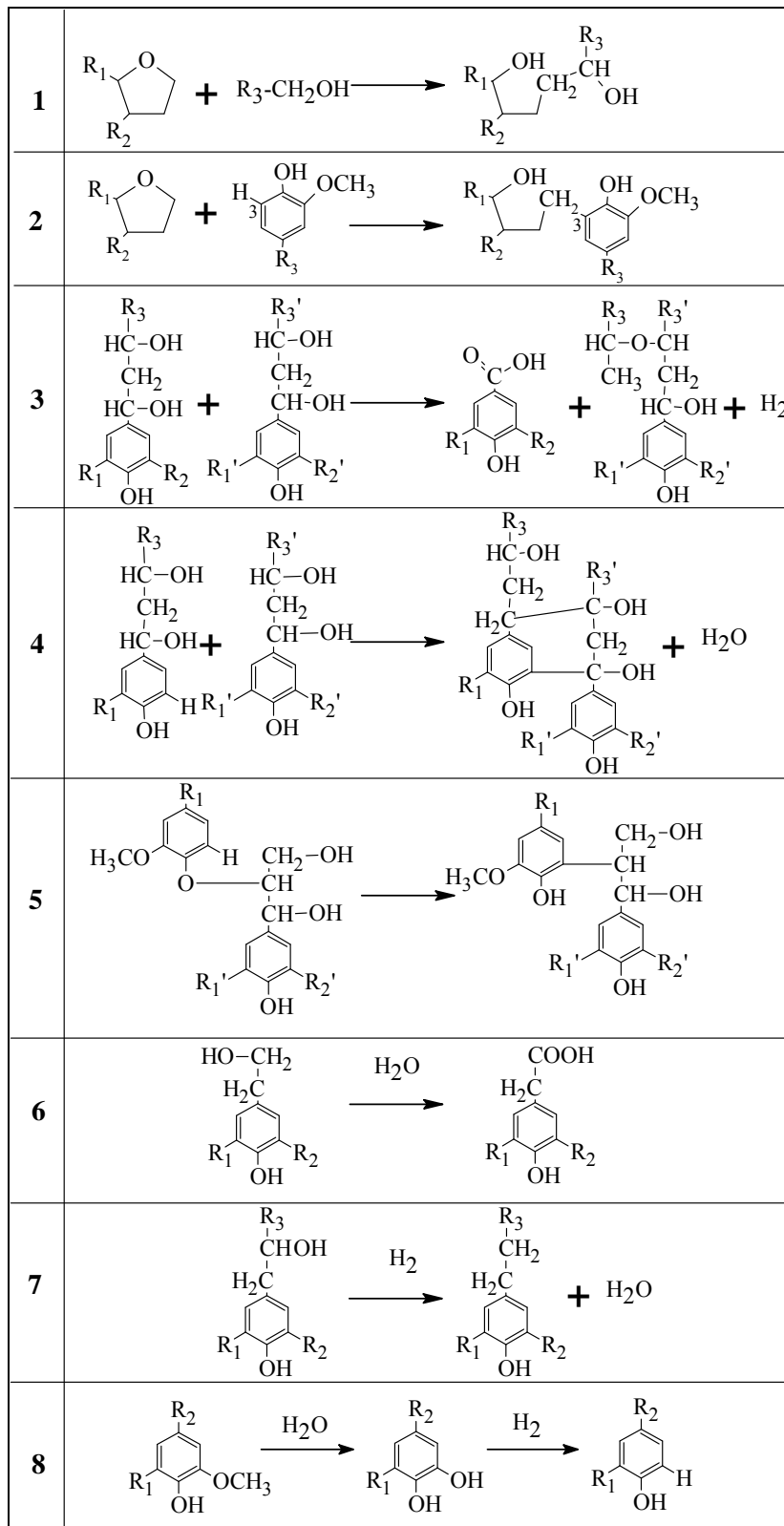
584

585

586

587 **Figure 2.** Early diagenesis reactions selected to transform the lignin structure to mature rank

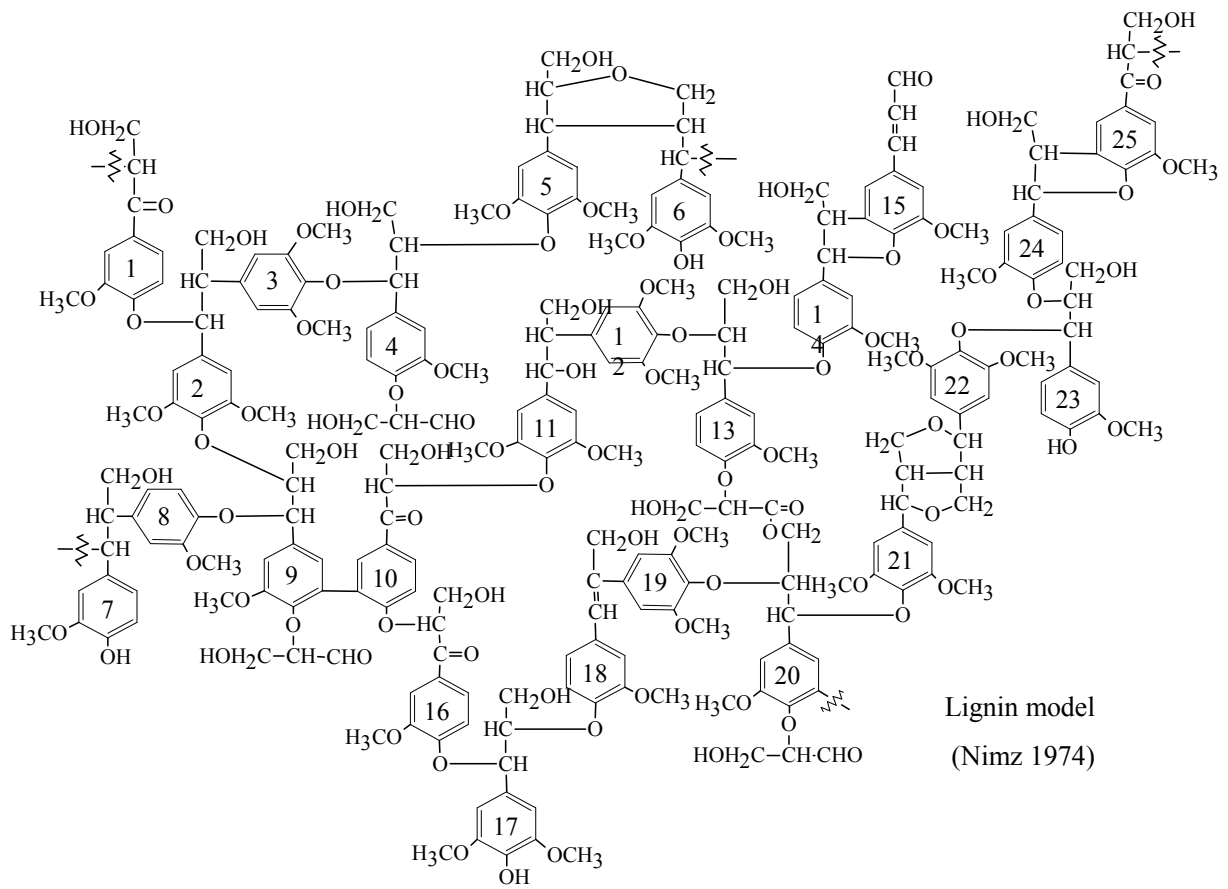
588 of lignite. (Hatcher, 1989; Hatcher and Clifford, 1997; Payne and Ortoleva, 2002)



589

590

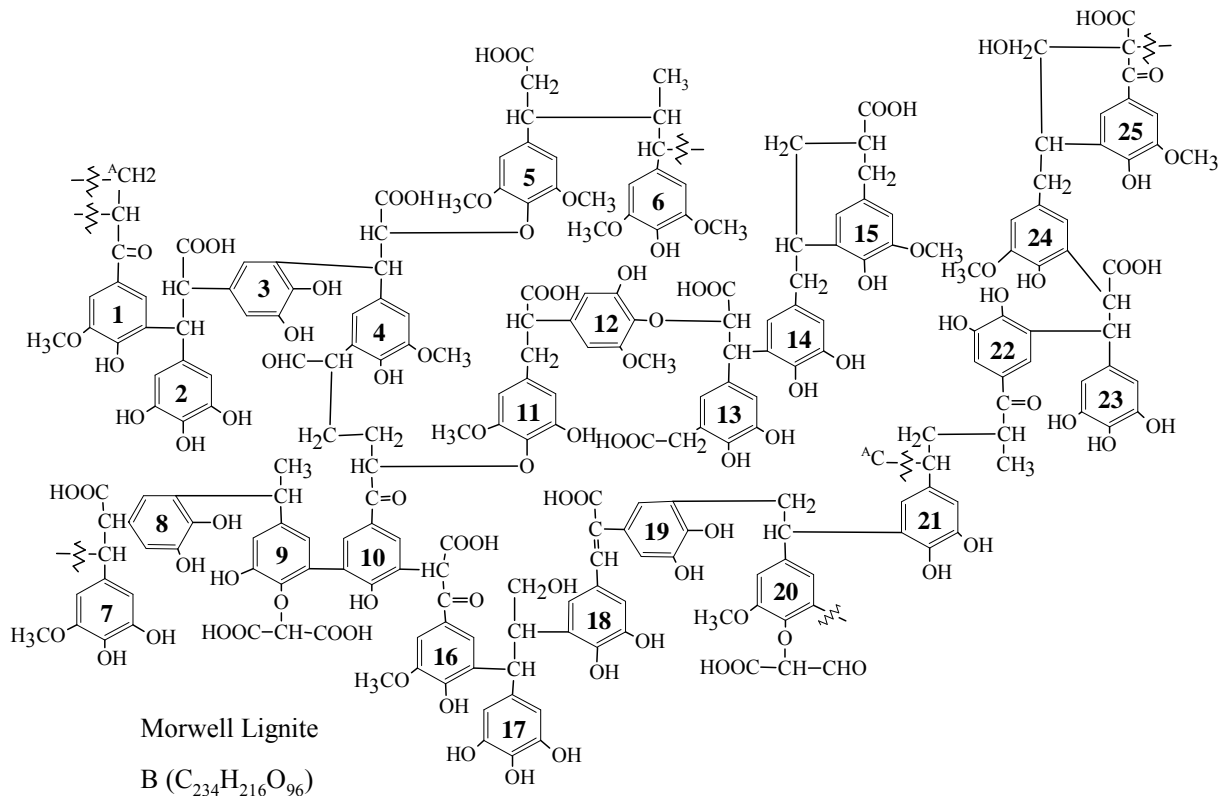
591 **Figure 3.** Beech lignin model from Nimz (1974)



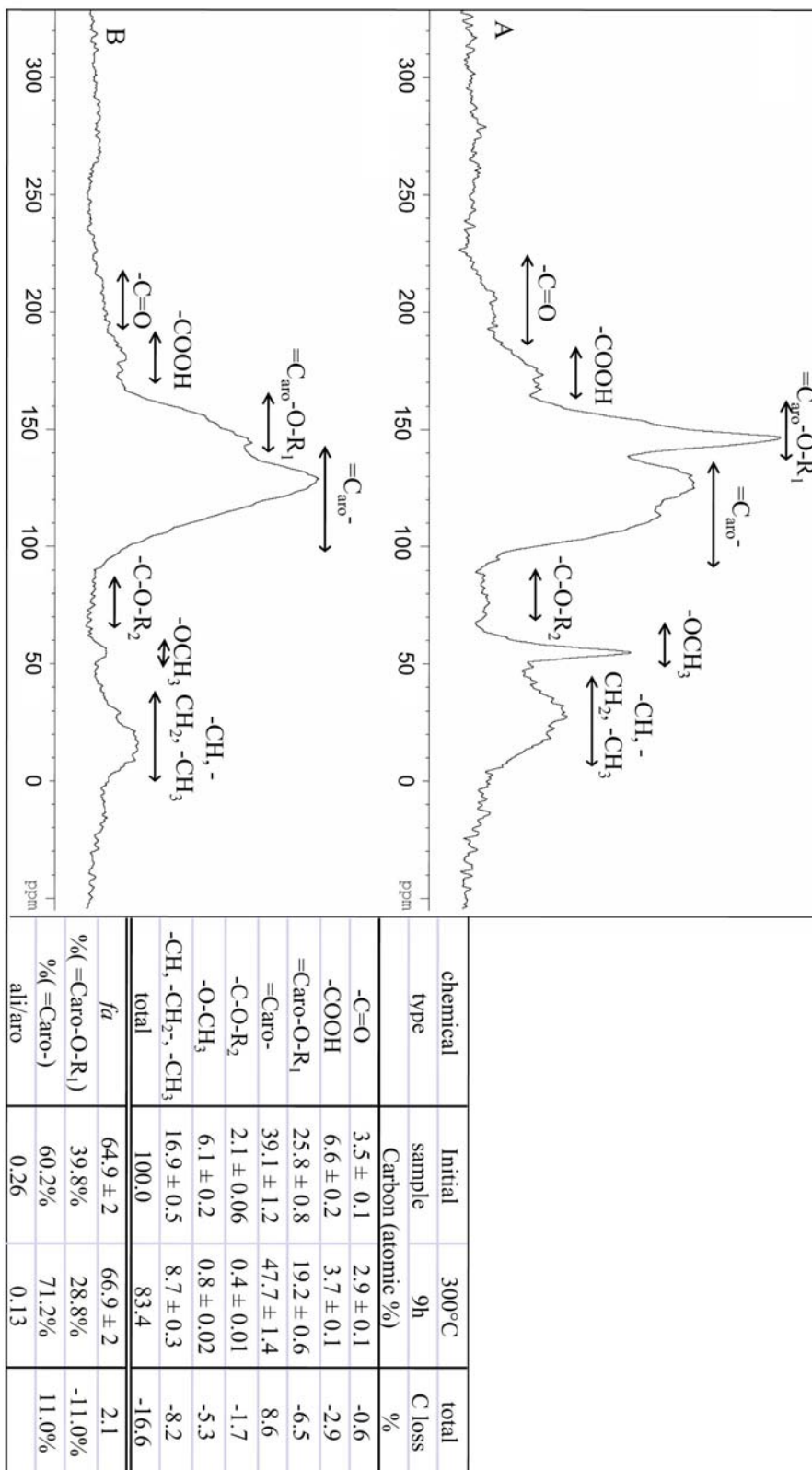
592

593

594 **Figure 4.** Structural model of the Morwell sample at coal rank of lignite.



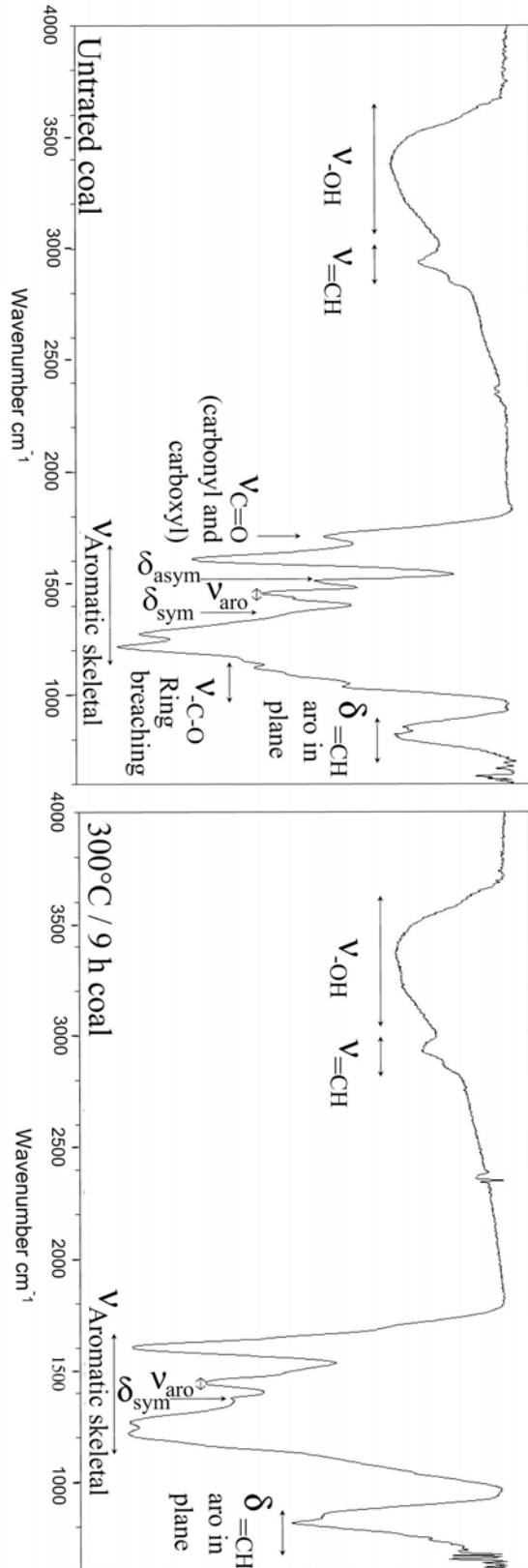
596 **Figure 5.** DPMAS ^{13}C NMR data of the initial sample of Morwell lignite (A) and residue (B)
 597 recovered after thermal stress (300 °C/9 h). The inset table provides quantitative
 598 measurements of the relative contributions of the various carbons. The % loss of carbon
 599 during artificial maturation is also indicated. The errors (\pm) are given for each calculated value
 600 and represent a relative error of 3% for peak area measurements.



601

602

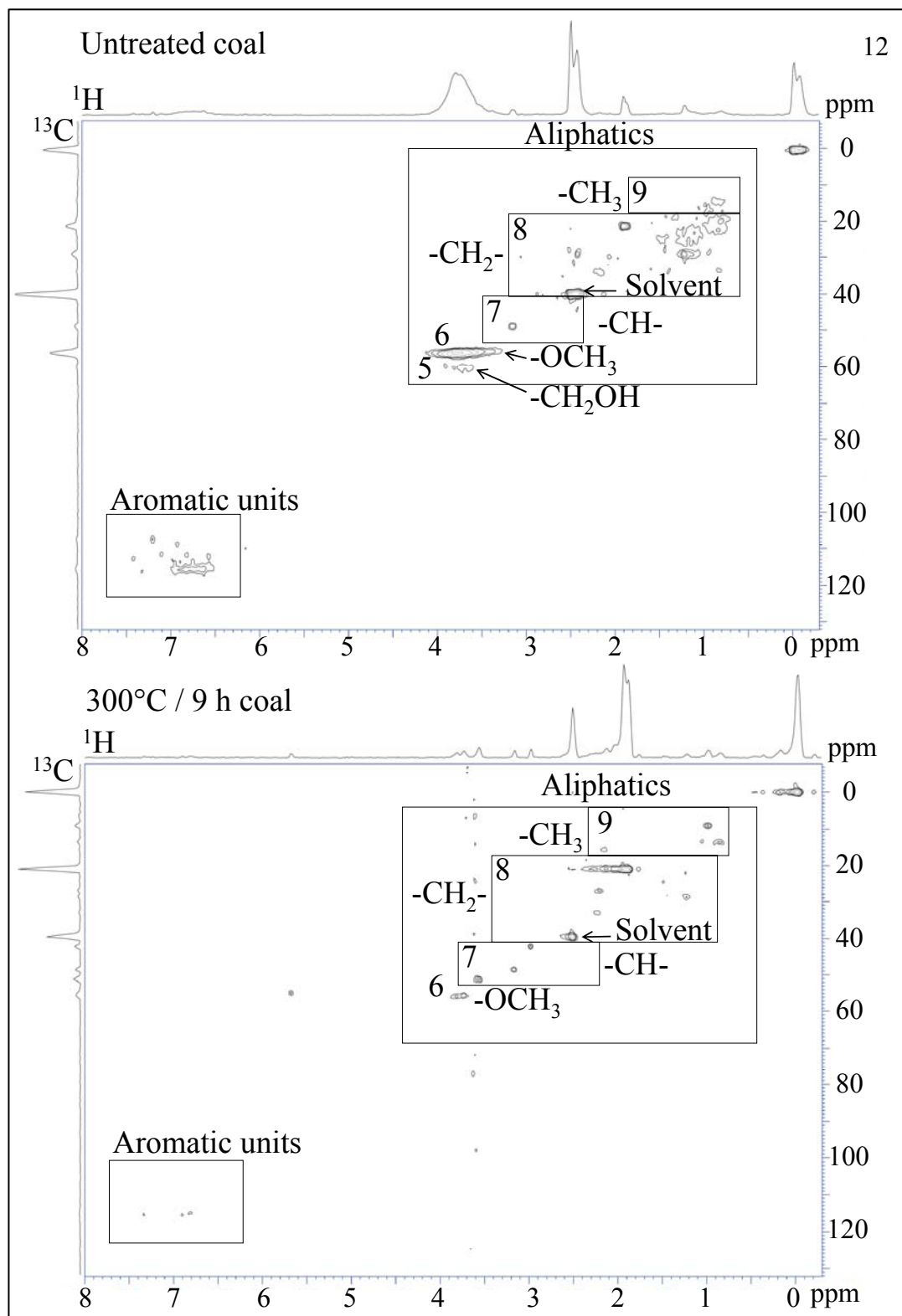
603 **Figure 6.** FTIR spectra of the initial sample of Morwell lignite (A) and the residue (B)
 604 recovered after thermal stress (300°C/9h). Various assignments for stretching (ν) and
 605 deformation (δ) frequencies.



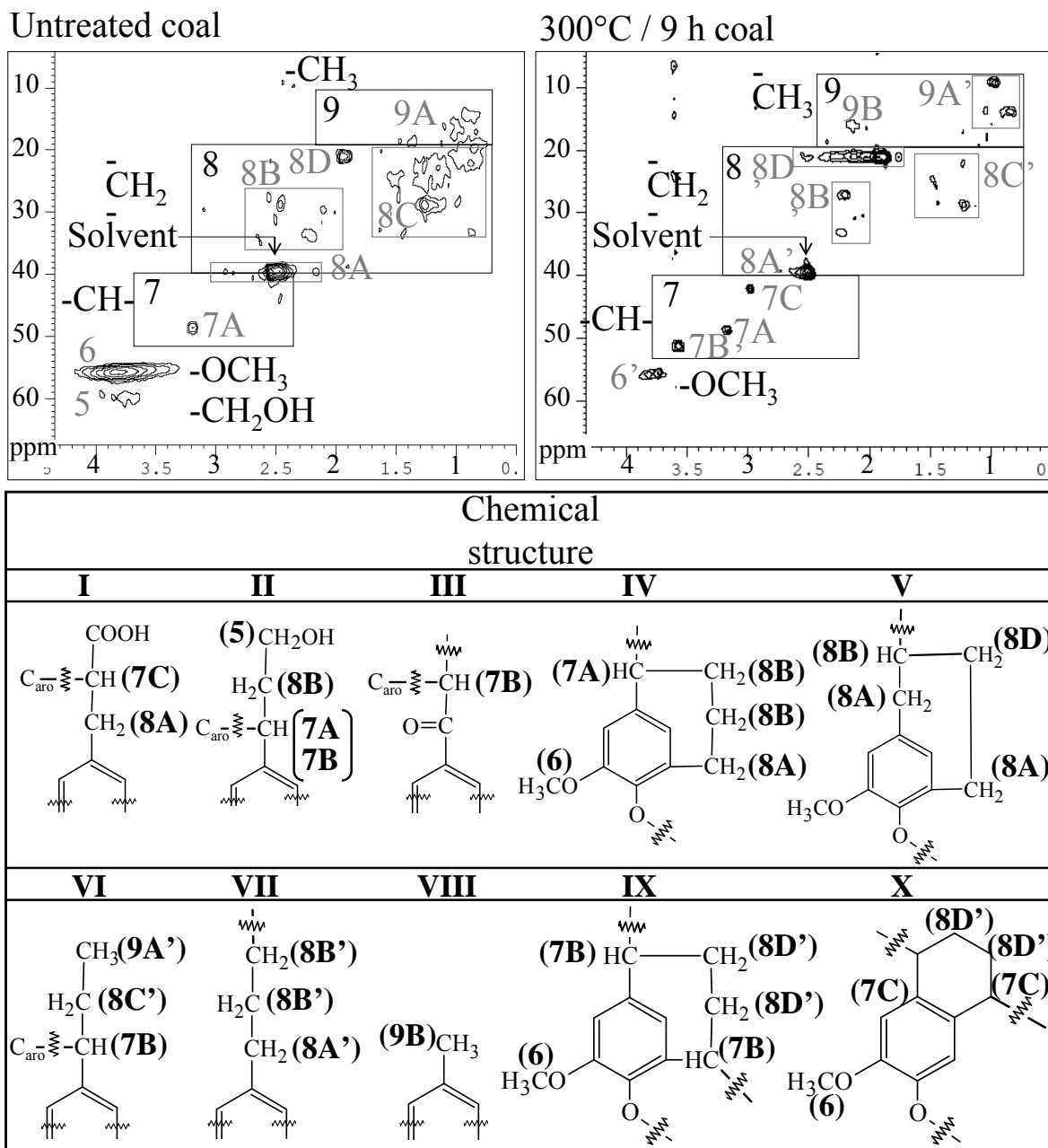
606
 607

608 **Figure 7.** HSQC spectra of the initial sample of Morwell lignite and the residue recovered after
609 thermal stress (300 °C/9 h). Boxed out regions are discussed in the text. The solvent peak is for
610 DMSO. The left ordinate projection is the respective DPMAS ¹³C NMR spectrum.

611

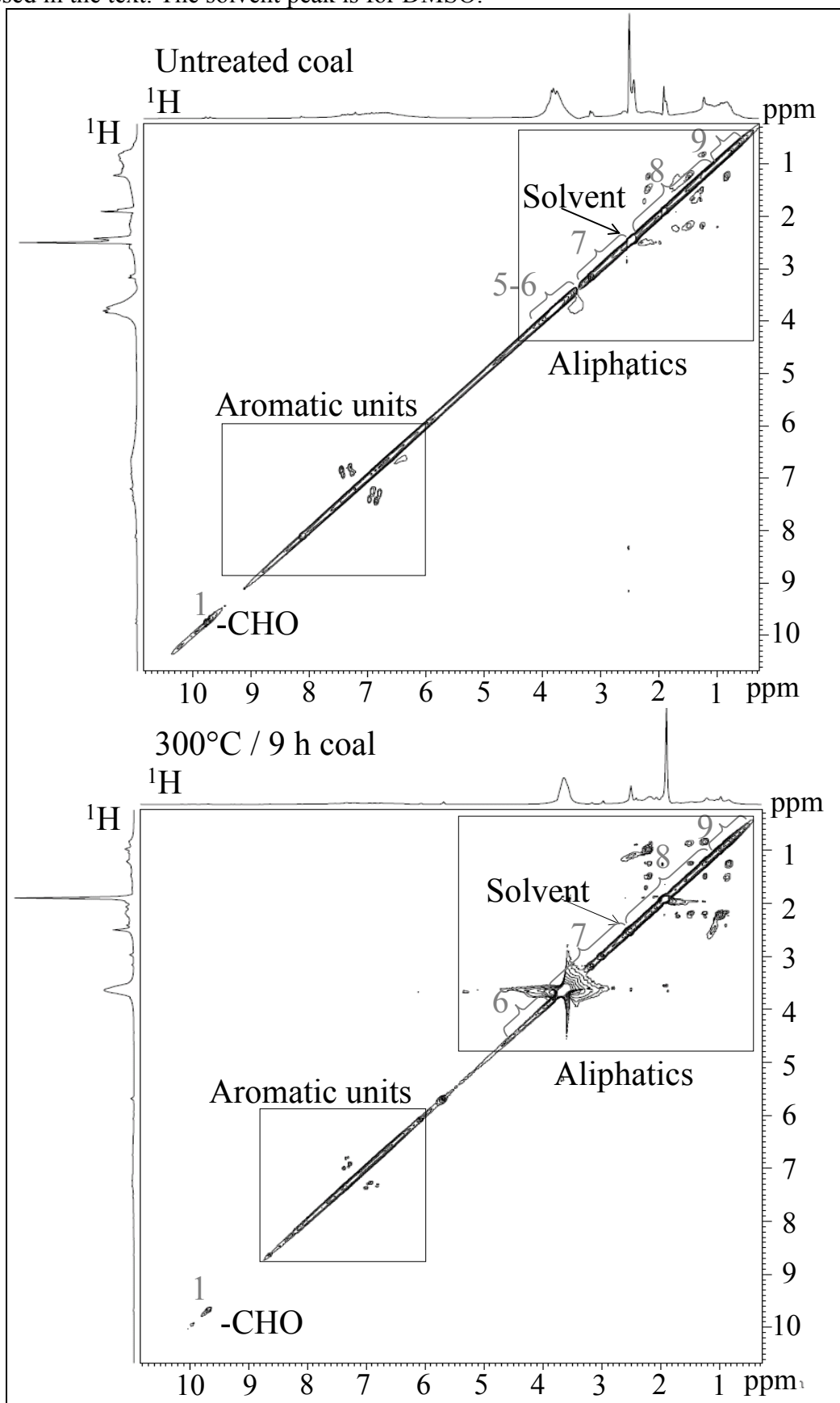


613 **Figure 8.** Extended aliphatic region of the HSQC NMR spectra in Figure 9 of the initial
 614 Morwell lignite and the residue recovered at 300°C/9 h. Structural assignments for the indicated
 615 carbon are presented in a table below of the spectra.

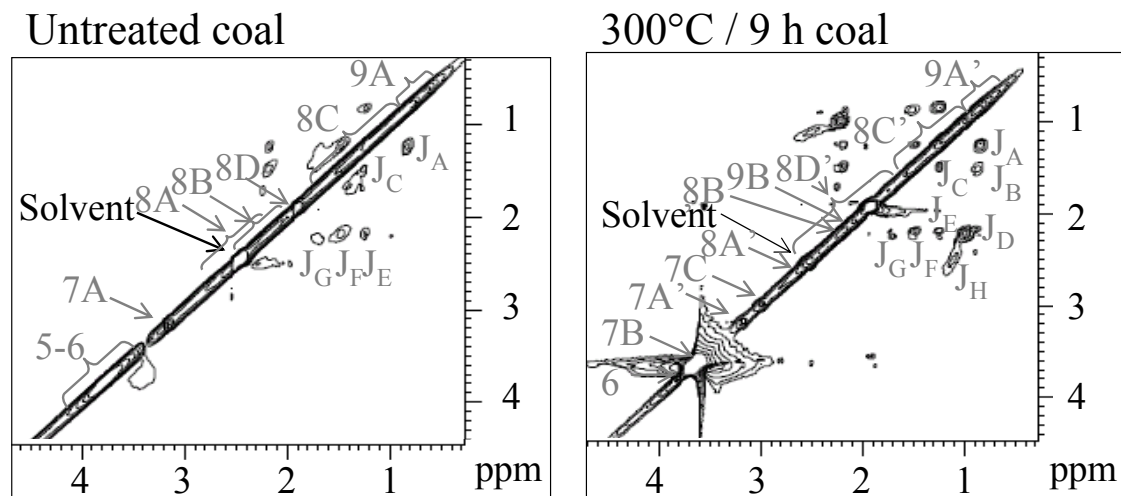


616

617 **Figure 9.** TOCSY spectra of the initial Morwell lignite and the residue recovered at 300°C/9
618 h. Structural assignments for some cross peaks are listed in Figure 8. Boxed out regions are
619 discussed in the text. The solvent peak is for DMSO.



621 **Figure 10:** Expanded view of the TOCSY spectrum in Figure 9. Structural assignments for the
 622 ^1H s are presented in a table below of the data with chemical shifts indicated for each coupled
 623 system.



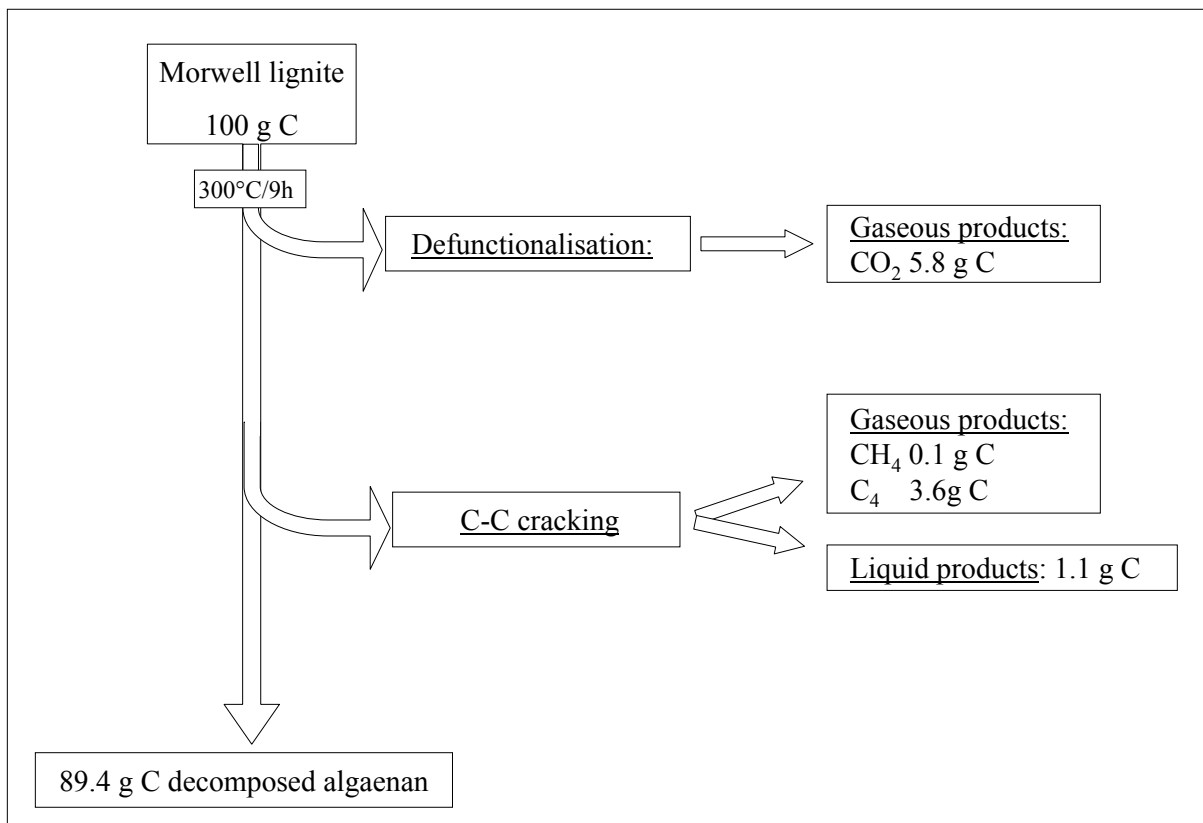
Chemical structure	Assignment coupling	Assignment carbons	$\delta^1\text{H}$	
			H_x	H_y
			ppm	
$\begin{array}{c} \text{CH}_3 \mathbf{a}_0 \\ \\ \text{CH}_2 \mathbf{a}_1 \\ \\ \text{H}_2\text{C} \mathbf{a}_2 \\ \\ \text{CH}_2 \mathbf{a}_3 \\ \\ \text{C}=\text{C} \end{array}$	J_A	$\mathbf{a}_0\text{-}\mathbf{a}_1, \mathbf{b}_0\text{-}\mathbf{b}_1, \mathbf{d}_0\text{-}\mathbf{d}_2$	0.8	1.3
$\begin{array}{c} \text{CH}_3 \mathbf{b}_0 \\ \\ \text{H}_2\text{C} \mathbf{b}_1 \\ \\ \text{CH}_2 \mathbf{b}_2 \\ \\ \text{C}=\text{C} \end{array}$	J_B	$\mathbf{a}_0\text{-}\mathbf{a}_2, \mathbf{b}_0\text{-}\mathbf{b}_2, \mathbf{d}_0\text{-}\mathbf{d}_1$	0.8	1.5
$\begin{array}{c} \text{CH}_3 \mathbf{c}_0 \\ \\ \text{CH}_2 \mathbf{c}_1 \\ \\ \text{C}=\text{C} \end{array}$	J_C	$\mathbf{a}_1\text{-}\mathbf{a}_2, \mathbf{b}_1\text{-}\mathbf{b}_2, \mathbf{d}_1\text{-}\mathbf{d}_2$	1.2	1.5
$\begin{array}{c} \mathbf{d}_0 \text{ CH}_3 \\ \\ \mathbf{d}_1 \text{ HC} \text{---} \text{CH}_2 \mathbf{d}_2 \\ \\ \mathbf{d}_2' \text{ CH}_2 \\ \\ \text{C}_6\text{H}_4 \text{---} \text{CH}_2 \mathbf{d}_3 \\ \\ \text{H}_3\text{CO} \text{---} \text{O} \end{array}$	J_D	$\mathbf{d}_0\text{-}\mathbf{d}_2'$	1.0	2.2
	J_E	$\mathbf{a}_1\text{-}\mathbf{a}_3, \mathbf{b}_0\text{-}\mathbf{b}_2$	1.2	2.2
	J_F	$\mathbf{d}_2\text{-}\mathbf{d}_3, \mathbf{d}_2\text{-}\mathbf{d}_2'$	1.5	2.2
	J_G	$\mathbf{d}_1\text{-}\mathbf{d}_2', \mathbf{d}_1\text{-}\mathbf{d}_3$	1.7	2.2
	J_H	$\mathbf{c}_0\text{-}\mathbf{c}_1$	1.1	2.6

624

625

626

627 **Figure 11.** Carbon mass balance of the Morwell lignite sample during 300°C/9h closed pyrolysis.



628